JCTC Journal of Chemical Theory and Computation

Classical Trajectory-Based Tunneling Splittings: The Hydrogen Atom Transfer in the Hydroperoxyl Anion

Kai Giese and Oliver Kühn*

Institut für Chemie und Biochemie, Physikalische und Theoretische Chemie, Freie Universität Berlin, Takustr. 3, D-14195 Berlin

Received November 28, 2005

Abstract: The hydroperoxyl anion HO_2^- is one of the simplest examples for multidimensional hydrogen-atom transfer. This is reflected in the tunneling splittings, which have been theoretically predicted to be highly selective concerning the excitation of either the O−O stretching, the O−H stretching, or the H−O−O bending vibration. Using the available quantum mechanical spectrum up to 5000 cm^{-1}, we scrutinize the performance of a recently proposed trajectory-based method to calculate tunneling splittings (Giese, K.; Ushiyama, H.; Kühn, O. *Chem. Phys. Lett.* **2003**, *371*, 681). It is found that this new method is capable of reproducing the general behavior of the tunneling splittings rather well. Furthermore, for this particular system, the error shows a systematic trend, which suggests the applicability of a scaling correction that could be based on a small number of exact splittings.

1. Introduction

Tunneling is a ubiquitous phenomenon in reactions involving hydrogen atoms and its isotopes.[1,2] Being a fundamental quantum effect, it continues to provide an inspiration for developing approximate methods for the efficient calculation of tunneling splittings. The semiclassical Wentzel−Kramers−Brillouin (WKB) approximation is not only the oldest but also the most rigorous approach in this respect, and its one-dimensional formulation is well-established.[3] However, multidimensional WKB theory appears to be too demanding to be turned into a practical scheme,[4−7] and quasi-one-dimensional approximations are often used.[8] Degrees of freedom (DOF) orthogonal to a one-dimensional tunneling path are included, for instance, in instanton theory,[9] for which a number of successful implementations have been developed.[10−17] On the other hand, the revival of semiclassical methods in the time domain[18] triggered the development of trajectory-based approaches, for example, within the semiclassical initial value representation[19−21] or by using the concept of multiple spawning.[22]

An even simpler approach which has the advantage of being straightforwardly interfaced with ab initio on-the-fly molecular dynamics goes back to Makri and Miller (MM method;[23] for applications, see also refs 24−27). Here, the recipe for calculating a tunneling splitting consists of running an ensemble of classical trajectories in one of the minima of the potential. Whenever the projection of the momentum onto a *predefined* tunneling direction changes sign, the trajectory is continued as a straight line along the tunneling direction through the classically forbidden region.

Reasonable choices for the tunneling direction depend on the actual potential, for example, on the type of coupling between the reaction coordinate and the considered vibrational mode. Although several possibilities have been discussed,[23−25,28] in particular, straight-line tunneling paths can only perform reasonably if the coupling between the reaction coordinate and vibrational mode is small.[29] Following the classification of the configuration space according to the solutions of the Hamilton−Jacobi equations, the action S can be real (R), imaginary (I), or complex (C) (see, e.g., ref 6 and Figure 1), and considering a simple two-dimensional symmetric mode coupling potential, the MM method based on straight-line paths connecting the minima and parallel to the reaction coordinate will perform best if tunneling goes through the C region. When tunneling mainly goes through the I region, the MM method will fail.

Recently, an extension of the MM method (called EMM) has been proposed,[29] which is based on the concept of tunneling trajectories developed by Takatsuka and co-

* Corresponding author fax: +49083854792; e-mail: ok@chemie.fu-berlin.de.

10.1021/ct0502918 CCC: $33.50
Published on Web 03/18/2006

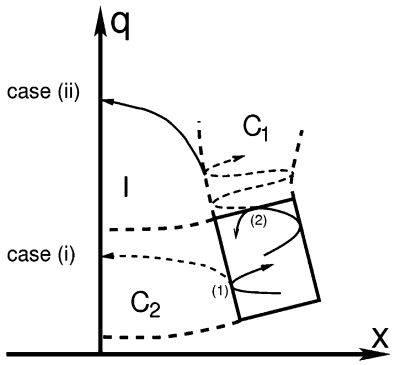

Figure 1. Illustration of the EMM method for a symmetric two-dimensional (x, q) potential and two turning points (1 and 2) leading to tunneling through the C (case i) and I (case ii) regions, respectively.

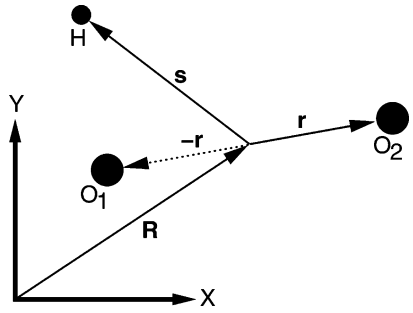

Figure 2. Definition of coordinates used for the hydroperoxyl anion (see text). The geometrical parameters as obtained by Chan and Hamilton using the QCISD(T)/6-311++G(2df,pd) method are $R_{HO} = 0.9619$ Å (1.1491 Å), $R_{OO} = 1.527$ Å (1.6991 Å), and $\gamma = 97.34°$ (42.3°) for the minimum (transition state)[32] (the figure is not to scale). The barrier height for hydrogen atom transfer is 71 kJ/mol (5941 cm^{-1}).

workers.[30] For the case of the above-mentioned two-dimensional symmetric mode coupling potential, it was shown that EMM outperforms MM in the case of strong couplings. This is possible because the tunneling is not restricted to occur along a predefined path. The aim of the present paper is to extend our previous model study and apply the EMM method to a real molecular system, that is, the hydroperoxyl anion, HO_2^-.

Among the nonrigid triatomics of the form HX_2, the hydroperoxyl anion has a rather low barrier for hydrogen-atom transfer and the distances of heavy atoms differ considerably between the C_s minimum and the C_{2v} saddle point geometry (see caption to Figure 2). Therefore, the minimum-energy path has a large curvature, which is an indication of a truly multidimensional transfer process. Chan and Hamilton[31,32] obtained an accurate potential energy surface using the QCISD(T)/6-311++G(2df,pd) level of quantum chemistry. The parameters of the relevant geometries are given in Figure 2. The lowest vibrational eigenstates were obtained by the same authors using a combination of a discrete variable representation and a Lanzcos diagonalization (in the following, denoted QM, see Table 1). The fundamental transitions are at 3575.1 cm^{-1} (O−H stretch), 1066.7 cm^{-1} (H−O−O bend), and 709.8 cm^{-1} (O−O stretch). The tunneling splittings are considerably mode-specific: For instance, for the O−O stretch fundamental transition, the splitting is 2×10^{-4} cm^{-1}, while for a combination excitation with one quanta, respectively, in the O−O stretch and H−O−O bend, it is 1×10^{-2} cm^{-1}. Thus, the hydroperoxyl anion appears to be very well-suited as a test case for the newly developed EMM method, because the tunneling splittings differ by orders of magnitude among different eigenstates.

Table 1. Mode Specific Tunneling Splittings ΔE of the Hydroperoxyl Anion[a]

	$E_n^{\pm}/hc$ (cm^{-1})		Δ_n/hc (cm^{-1})		
state	+	−	QM	MM	EMM
(0,0,0)	0	0		0.000 03	0.000 02
(0,0,1)	709.8	709.8	0.0002	0.000 04	0.0003
(0,1,0)	1066.7	1066.7	0.0009	0.001	0.004
(0,0,2)	1408.7	1408.7	0.001	0.0001	0.002
(0,1,1)	1753.4	1753.4	0.01	0.01	0.03
(0,2,0)	2084.3	2084.3	0.03	0.1	0.2
(0,0,3)	2092.5	2092.5	0.004	0.0007	0.007
(0,1,2)	2426.2	2426.3	0.08	0.1	0.1
(0,2,1)	2745.3	2745.6	0.3	1.2	1.1
(0,0,4)	2756.8	2756.8	0.02	0.005	0.03
(0,3,0)	3063.5	3064.1	0.6	3.4	2.8
(0,1,3)	3081.2	3081.5	0.3	0.9	0.7
(0,2,2)	3388.2	3390.2	2.0	7.1	5.6
(0,0,5)	3398.9	3399.1	0.2	0.06	0.2
(0,3,1)	3692.5	3698.3	5.8	10.3	9.9
(0,1,4)	3714.9	3716.1	1.2	3.9	3.2
(0,4,0)	4000.4	4011.0	10.6	14.2	13.5
(0,2,3)	4010.6	4013.5	2.9	10.4	9.2
(0,0,6)	4017.1	4020.0	2.9	0.3	0.6
(0,3,2)	4285.0	4316.4	31.4	10.1	9.5
(0,1,5)	4323.9	4328.1	4.3	8.9	6.7
(0,4,1)	4562.1	4606.9	44.8	9.9	9.2
(0,2,4)	4600.0	4620.9	20.9	10.8	8.6
(0,0,7)	4608.3	4624.3	16.0	1.6	2.4
(0,5,0)	4826.9	4916.3	89.4	7.7	7.4
(0,3,3)	4895.2	4919.6	24.4	6.1	5.0
(0,1,6)	4907.2	4931.4	24.2	9.5	8.9
(0,1,6)	4907.2	4931.4	24.2	.5	8.9

[a] The values $E_n^{\pm}$ and the quantum mechanical (QM) splittings Δ_n are taken from ref 32.

The paper is organized as follows: In section 2, we will first give a brief review of the EMM method. We continue by discussing the specific implementation of MM and EMM strategies for the case of HO_2^-. The results obtained for both methods are compared to the numerically exact quantum mechanical data in section 3. We summarize in section 4.

2. Theory

2.1. The EMM Method. Before we review the EMM approach, let us briefly recall the MM method.[23] Here, an ensemble of classical trajectories is propagated in the classically allowed region in the neighborhood of a minimum of the potential $V(\mathbf{q})$. If at time t_n the projection of the momentum $\mathbf{p}$ onto a tunneling direction $\mathbf{d}$ changes sign, a turning point is reached and the trajectory is continued as a straight line in the classically forbidden region. Denoting this turning point $\mathbf{q}_n^*$, the tunneling probability for an individual trajectory at time t is given by (in mass-weighted coordinates)

$$P(t) = \sum_{t \le t_n} \exp\left(-\frac{1}{\hbar} \int_0^{\xi_{max}} d\xi \sqrt{2[V(\mathbf{q}_n^* + \xi \mathbf{d}) - V(\mathbf{q}_n^*)]} \right) \quad (1)$$

where ξ_{max} is the maximum length of the straight-line path for which the square root is real. The tunneling splitting is then given by

$$\Delta = 2\hbar \frac{d}{dt}\langle P(t)\rangle \tag{2}$$

where $\langle ... \rangle$ denotes the ensemble average.

While this approach involves an a priori definition of a tunneling direction, which is usually taken as a straight-line path, the EMM method does not have such constraints. Here, the trajectories are propagated, and a parity of motion, $\sigma_j = \pm 1$, is assigned to each DOF such that real-valued momenta can always be defined via[30]

$$\bar{p}_j = p_j/\sqrt{\sigma_j} \tag{3}$$

For $\sigma_j = +1$ and $\sigma_j = -1$, the motion is classically allowed and forbidden, respectively. Note that transformation eq 3 is noncanonical if $\sigma_j = -1$. Inserting eq 3 into the usual Hamiltonian yields

$$\bar{H}(\bar{\mathbf{p}},\mathbf{q};\sigma) = \sum_j \frac{\sigma_j}{2}\bar{p}_j^{\,2} + V(\mathbf{q}) \tag{4}$$

where $\sigma = (\sigma_1,...,\sigma_N)$ is the vector of parities of motion. Trajectories in the $(\bar{\mathbf{p}},\mathbf{q})$ space can be generated by Hamilton's equation of motion

$$\dot{p}_j = -\frac{\partial \bar{H}}{\partial q_j} = -\frac{\partial V}{\partial q_j} \tag{5}$$

$$\dot{q}_j = \frac{\partial \bar{H}}{\partial \bar{p}_j} = \sigma_j \bar{p}_j \tag{6}$$

The first equation, eq 5, is the unchanged Newton's equation of motion. However, the second equation, eq 6, determines that, for $\sigma_j = -1$, the velocity $\dot{q}_j$ and momentum $\bar{p}_j$ have opposite directions. Notice that eqs 5 and 6 are equivalent to the formulation in ref 30 and have a canonically invariant form. This implies that the method of characteristics can be used to construct an action function based on a field of trajectories.[33] However, for the present purpose, we define the action along a trajectory on a σ sheet (for constant energy) by

$$S(\bar{\mathbf{p}}_0,\mathbf{q}_0,\sigma;t) = \sum_j \int_0^t \sqrt{\sigma_j}\,\bar{p}_j(\tau)\,\dot{q}_j(\tau)\,\mathrm{d}\tau \tag{7}$$

where $(\bar{\mathbf{p}}_0,\mathbf{q}_0)$ are the initial conditions of the trajectory. As was noted before, the transformation eq 3 is noncanonical; that is, trajectories generated for different sets of parities σ refer to different dynamical systems, and it is necessary to resort to intuitive arguments in order to connect solutions belonging to different sheets.

The calculation of tunneling splittings in the EMM approach proceeds as follows: (i) Initial conditions for an ensemble in either the left or the right well are generated, for example, from normal-mode sampling.[25] (ii) A trajectory is propagated in the R region of the potential (see Figure 1) until it hits a classical turning point $\mathbf{q}_n^{(cl)}$. In ref 29, it was suggested that these turning points can be defined by the condition $\bar{\mathbf{p}}\cdot\mathbf{d}_i = 0$, where $\{\mathbf{d}_i\}$ is a set of tunneling directions which is defined by the normal-mode vectors of the potential minimum. (iii) Whenever a trajectory encounters such a turning point, the parity σ_j of the corresponding direction $\mathbf{d}_j$ is flipped from $+1$ to -1 and the propagation is continued according to the eqs 5 and 6. The turning point condition is also used to determine *nonclassical* turning points outside the R region: When the turning point condition is fulfilled for a trajectory in the forbidden region, then another parity σ_k of the corresponding direction is flipped from $+1$ to -1. Both trajectories in the forbidden region, the one with $\sigma_j = -1$ and $\sigma_k = +1$ as well as the one with $\sigma_j = -1$ and $\sigma_k = -1$, will be integrated in this case (see Figure 1). The extension to more than two dimensions is straightforward. (iv) When a trajectory that is propagated in the forbidden region crosses the symmetry line Σ, the complex action of that trajectory is computed. The action is given by the integral eq 7 along the trajectory from $\mathbf{q}_n^{(cl)}$ to the crossing point on the symmetry line. There may be several trajectories that emanate from one classical turning point $\mathbf{q}_n^{(cl)}$. Only the action that has the smallest imaginary part is kept, and its absolute value is denoted W_n. (v) The contributions of all nonclassical trajectories with the smallest action that have emanated from classical turning points $\mathbf{q}_n^{(cl)}$ at time t_n are summed up according to

$$P(t) = \sum_{t_n \le t} \exp\left(-\frac{2}{\hbar}W_n\right) \tag{8}$$

from which the splitting is obtained via eq 2. For more details, we refer to the original publication[30] as well as to the earlier paper on the EMM method.[29]

2.2. Implementation for HO_2^-. Both methods, MM and EMM, are formulated in Cartesian coordinates. For MM, this is because the straight-line paths are defined as Cartesian vectors; for EMM, the parities of motion are associated with Cartesian momenta. Recently, Guo and Thompson[28] applied the MM approach to hydrogen peroxide (HOOH) and used the torsional angle as the tunneling coordinate instead of a straight line. This was possible because a single internal coordinate was (assumed to be) responsible for the tautomerization. However, a generalization seems to be hardly possible when more internal non-Cartesian coordinates have to be considered. To apply these methods to a case like the hydroperoxyl anion, it is therefore necessary to describe the molecule in a Cartesian coordinate system.

First, we notice that two rotational DOF can be removed by confining the motion to a plane. For the remaining DOF, the coordinate vectors **R**, **r**, and **s**, as defined in Figure 2, are employed. The positions of the two oxygen atoms, $\mathbf{r_1}$ and $\mathbf{r_2}$, and the position of the hydrogen atom, $\mathbf{r}_3$, can be expressed as

$$\mathbf{r_1} = \mathbf{R} - \mathbf{r} \tag{9}$$

$$\mathbf{r_2} = \mathbf{R} + \mathbf{r} \tag{10}$$

$$\mathbf{r_3} = \mathbf{R} + \mathbf{s} \tag{11}$$

Assuming (without restriction) that the center of mass of the

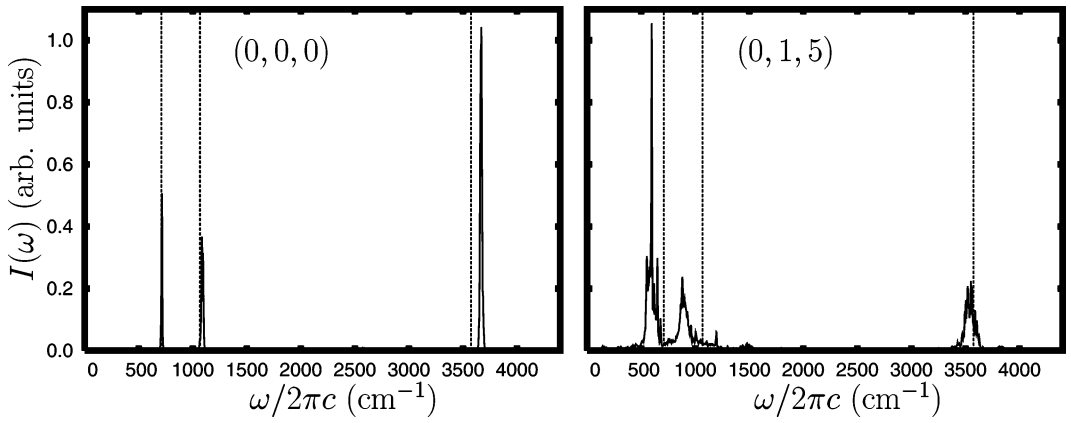

Figure 3. Power spectra $I(\omega)$ (cf. eq 14) for the ground state (0, 0, 0) and excited state (0, 1, 5). The power spectra were obtained by propagating ensembles of 100 trajectories and Fourier transformation of $Z(t) = \sum_i P_i(t)$ with Gaussian broadening $\exp\{-t^2/\tau^2\}$ and $\tau = 5$ ps. The propagation time was 14.5 ps. Fundamental transitions are indicated as dashed lines (cf. Table 1).

triatomic is fixed at the origin, it follows that

$$\mathbf{R} = -\frac{m_H}{M}\mathbf{s} \tag{12}$$

where m_H and M are the mass of a hydrogen and the total mass of the triatomic, respectively. The Lagrangian of the system can be derived straightforwardly as

$$\mathcal{L} = \frac{1}{2}m_H\left(1 - \frac{m_H}{M}\right)\dot{\mathbf{s}}^2 + \frac{1}{2}(2m_O)\dot{\mathbf{r}}^2 - V(\mathbf{s},\mathbf{r}) \tag{13}$$

where m_O is the oxygen mass and $V(\mathbf{s},\mathbf{r})$ is the potential energy surface. The configuration space $(\mathbf{s},\mathbf{r})$ of this Lagrangian is four-dimensional. This means that—because there are three internal coordinates—an individual trajectory is only unique up to an arbitrary rotation around the four-dimensional origin ($\mathbf{s} = 0$, $\mathbf{r} = 0$) corresponding to a rotation around the six-dimensional center of mass.

In the following, the vibrational eigenstates will be labeled as $\mathbf{n} = (n_1, n_2, n_3)$, where the quantum numbers correspond to the O−H stretch (n_1), H−O−O bend (n_2), and O−O stretch (n_3) vibrations. The initial conditions for the ensembles of trajectories corresponding to an eigenstate $\mathbf{n}$ were obtained by normal-mode sampling with energy rescaling,[25] where the energy was chosen to be the mean of the exact quantum mechanical energy for a split pair of levels. The normal-mode analysis with respect to a four-dimensional minimum, $(\mathbf{s}^{(\min)},\mathbf{r}^{(\min)})$, yields three vibrational normal modes plus an infinitesimal rotational vector. The normal modes are only guaranteed to be orthogonal to the infinitesimal rotational vector that corresponds to the minimum; for a displaced geometry, there is a slightly different rotational vector. Therefore, for each trajectory, the angular momentum was removed, and in order to keep the energy fixed, the momenta were rescaled.

To assess the quality of the initial state sampling, we have calculated power spectra of the sum of momenta $Z(t) = \sum_i P_i(t)$:

$$I(\omega) = \frac{1}{2\pi}\lim_{T\to\infty}\frac{1}{T}\langle|\int_0^T \mathrm{d}t\, Z(t)\exp(-i\omega t)|^2\rangle \tag{14}$$

where the brackets indicate an averaging over an ensemble of classical trajectories. Exemplary spectra for the ground state (0, 0, 0) at a total energy of 2676 cm^{-1} and state (0, 1, 5) at a total energy of 7000 cm^{-1}, respectively, are shown in Figure 3. The state (0, 1, 5) was chosen as being typical for a highly excited state. In both spectra, one may identify three main peaks that correspond to quasi-periodical motion with the three fundamental frequencies. For the ground-state spectrum, these peaks are narrow, indicating that phase space points on (or very close to) a certain invariant torus are sampled.[34] A comparison with the exact quantum mechanical fundamental transitions (dashed vertical lines) shows that this invariant torus almost coincides with the ground-state invariant torus. Conversely, in the spectrum of state (0, 1, 5), the main peaks are broadened and possess a substructure. The significant shifts of the peak maxima with respect to the quantum mechanical fundamentals are due to the anharmonicity of the potential. Thus, for the state (0, 1, 5), one expects the normal-mode sampling to be less efficient. Nevertheless, the appearance of three distinct peaks indicates that an invariant torus corresponding to the quantum state exists at least approximately.

For the MM method, the tunneling direction is defined such that the O−O distance vector $2\mathbf{r}$ is held fixed for the tunneling process; that is, at each point $(\mathbf{s},\mathbf{r})$, the tunneling direction could be calculated from

$$\mathbf{d}_{MM} = \begin{pmatrix}\mathbf{r}/|\mathbf{r}|\\ 0\end{pmatrix} \tag{15}$$

a choice which was also used for malonaldehyde in refs 24 and 26. If the hydrogen would be located in the left well (i.e., $\mathbf{s}\cdot\mathbf{r} < 0$), then a straight line along $\mathbf{d}_{MM}$ leads automatically to a C_{2v} configuration of the triatomic. This configuration is a point on the symmetry surface Σ that is defined by $\mathbf{s}\cdot\mathbf{r} = 0$ in the present case.

However, the molecule will rotate along a straight line defined by Cartesian directions as given by eq 15. This is because only the hydrogen moves along these straight lines, and the complementary counter rotation of the O−O axis is missing. Because of the mass ratio of about 1:16 between hydrogen and oxygen, the error introduced by the straight-

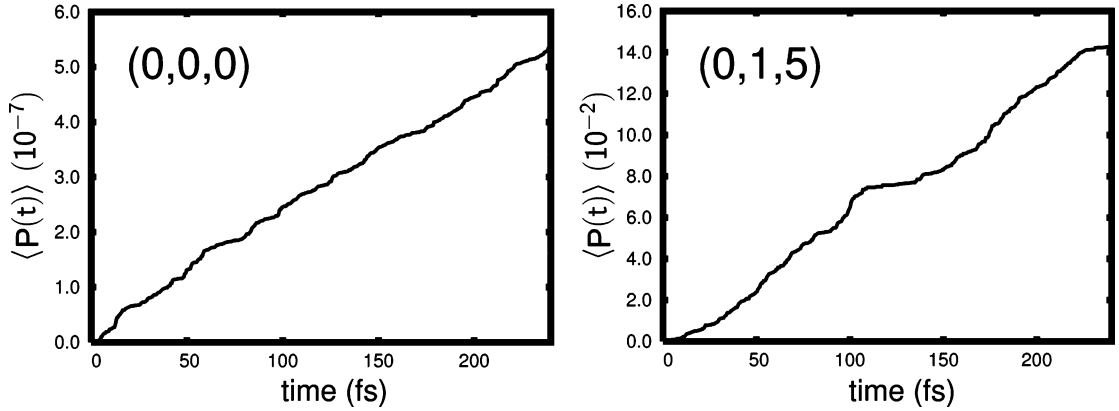

Figure 4. Cumulated EMM tunneling probabilities $\langle P(t)\rangle$ (ensemble of 1000 trajectories) for the ground state (0, 0, 0) and excited state (0, 1, 5).

line approximation may be small, although its magnitude is unknown a priori. However, a rotation-free tunneling direction and also a related rotation-free tunneling path can be constructed. To this end, let us consider a modified tunneling direction that is given by

$$\mathbf{d}_{\mathrm{MM}}^{\mathrm{R}} = \frac{\mathbf{d}_{\mathrm{MM}} - (\mathbf{d}_{\mathrm{MM}}\rho)\rho}{|\mathbf{d}_{\mathrm{MM}} - (\mathbf{d}_{\mathrm{MM}}\rho)\rho|} \tag{16}$$

where $\rho = \rho(\mathbf{s}_1,\mathbf{r}_1)$ is the infinitesimal rotational vector at the (turning) point $(\mathbf{s}_1,\mathbf{r}_1)$. With definition eq 16, the rotation in the vicinity of the turning point is removed. A complete rotation-free path may be obtained by solving the ordinary differential equation:

$$\frac{\mathrm{d}\mathbf{X}}{\mathrm{d}\xi} = \mathbf{d}_{\mathrm{MM}}^{\mathrm{R}}[\mathbf{X}(\xi)] \tag{17}$$

where $\mathbf{X}(\xi)$ is a 4D vector as a function of the coordinate ξ along the curved path. The tunneling direction eq 16 is considered to be **X**-dependent, such that ρ is evaluated at each point on the path while $\mathbf{d}_{\mathrm{MM}}$ is held fixed.

However, it turned out that the correction to the tunneling splittings due to the rotation-free tunneling path, eq 17, is negligible for the present molecule. Therefore, the MM tunneling integral, eq 1, was computed by following a straight-line tunneling path defined by the rotation-free direction eq 16, and turning points are given by the zeros of $\mathbf{P}\cdot\mathbf{d}_{\mathrm{MM}}^{\mathrm{R}}$, where **P** is the four-dimensional momentum.

In analogy to eq 15, the EMM turning point condition was modified such that, for each point $(\mathbf{s},\mathbf{r})$, the set of vectors $\{\rho,\mathbf{d}_1,\mathbf{d}_2,\mathbf{d}_3\}$ is Schmidt-orthogonalized. Here, $\mathbf{d}_i$ corresponds to the normal-mode direction of the three fundamental vibrations at the minimum. The procedure guarantees that, for a turning point $\mathbf{P}\cdot\mathbf{d}_i' = 0$ with Schmidt-orthogonalized normal-mode vector $\mathbf{d}_i'$, the parity of motion is flipped to -1 for a direction that is orthogonal to the rotational direction at that turning point. The generalized trajectories are then generated for a reduced space that is spanned by the three Schmidt-orthogonalized normal-mode directions $\mathbf{d}_i'$. Notice that this is a generalization of the condition used for the MM tunneling directions and turning points. In particular, the straight line generated by direction eq 16 can be expressed as a linear combination of the $\mathbf{d}_i'$ values. The integration of a trajectory is stopped when the symmetry surface Σ has been reached, that is, when $\mathbf{s}\cdot\mathbf{r} \geq 0$.

For each vibrational level, **n** ensembles of 1000 classical trajectories were propagated using a fifth-order symplectic integrator[35] with a fixed step size of 0.48 fs. For the accurate determination of turning points, the step size was reduced to 0.048 fs. The propagation time was 240 fs, which corresponds to about 5 times the vibrational period of the weakest mode. The energy was bound within a typical maximum tolerance of 0.1 cm^{-1}.

In Figure 4, cumulated EMM tunneling probabilities $\langle P(t)\rangle$ for, respectively, the ground state (0, 0, 0) and state (0, 1, 5) are shown, which correspond to the power spectra in Figure 3. Compared to the ground state, there is an oscillation superimposed on the approximate linear increase of $\langle P(t)\rangle$ for state (0, 1, 5). This can be attributed to the sampling method; that is, the trajectories are only near the invariant torus.[25] Only those states are considered for which the linear regression of the data points yields a relative standard deviation of less than 1%. Notice that this excludes the states $(1, n_2, n_3)$ which show a larger deviation. The sampling error was estimated by performing five distinct runs for the (0, 0, 1) level; the relative standard deviation was 8% of the tunnel splitting.

3. Results

In Table 1, tunneling splittings obtained by diagonalizing the Hamiltonian (QM data taken from ref 32) are compared with semiclassical results obtained within, respectively, the MM and EMM approaches. When comparing the MM results for, for example, the fundamental of the O−O vibration (0, 0, 1) with those for the QM, one finds an underestimation of almost 1 order of magnitude. Conversely, the EMM result for that vibrational state agrees quite well with the QM. The same finding applies to overtones of the O−O vibration up to state (0, 0, 5). For the fundamental of the H−O−O bend vibration (0, 1, 0), the tunneling splittings are overestimated by the EMM. The same applies for states (0, 2, 0) and (0, 3, 0). Also, the MM yields too-large tunneling splittings for the two states (0, 2, 0) and (0, 3, 0). Finally, we note that, for the MM method, we have investigated the rotational error due to the use of a tunneling path which is not rotation-free for the lowest 10 states in Table 1. It turns out that, for the

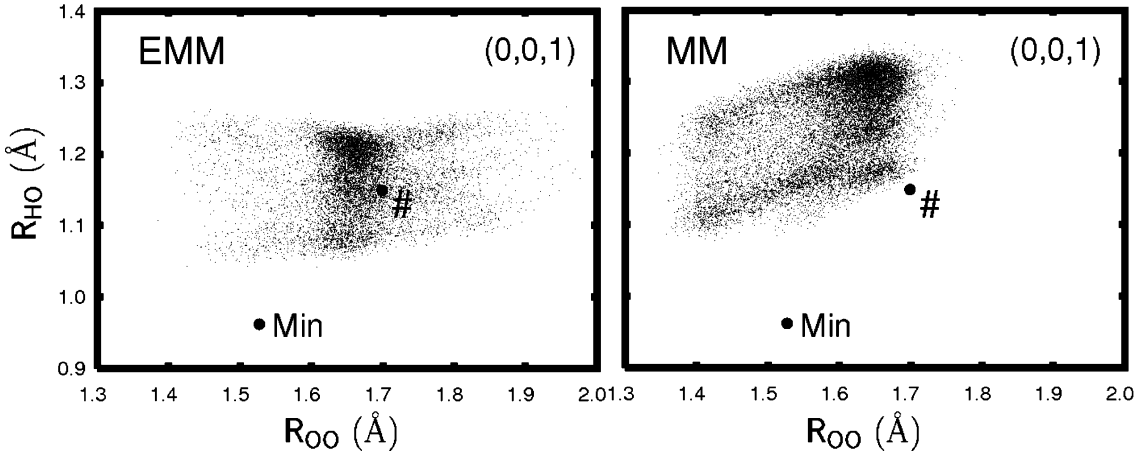

Figure 5. Point cloud plot of the tunneling probability, $\exp(-2W_n/\hbar)$, at the symmetry surface (C_{2v} configuration), where W_n is the absolute value of the imaginary part of the action obtained for a path from the nth turning point to the point (R_{HO}, R_{OO}) on the symmetry surface. The local density of points at (R_{HO}, R_{OO}) is chosen to be proportional to $\langle\sum_n (W_n)^{-4}\rangle$. The saddle point is indicated (#); the minimum is not a point on the symmetry surface, but the minimum bond length values are given for comparison and marked by "Min".

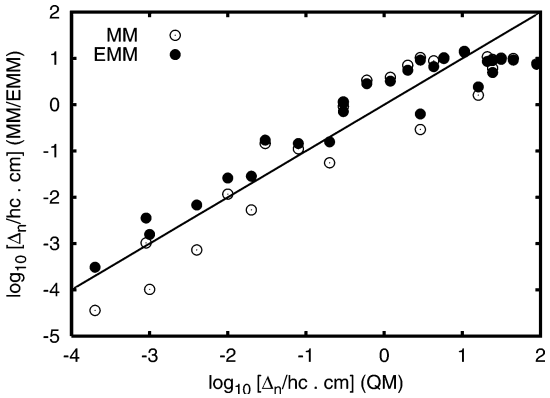

Figure 6. Mode-specific tunneling splittings Δ_n (logarithmic). Values obtained by MM and EMM vs the exact QM result. The solid line corresponds to perfect agreement.

reported number of digits, only for state (0,0,3) does the tunneling splitting change (to 0.0008 cm^{-1}).

In Figure 5 the magnitude of the tunneling action W_n at the symmetry surface Σ is visualized for the state (0, 0, 1) by point-cloud plots for EMM and MM. For visual clarity, the local density of points has been chosen to be proportional to $\sum_n W_n^{-4}(R_{HO}, R_{OO})$: a higher density corresponds to smaller action and, thus, a larger tunneling probability. For state (0, 0, 1), the maximum of the EMM and MM is at (R_{HO}, R_{OO}) $\approx$ (1.2, 1.65) Å and (1.3, 1.65) Å, respectively. Thus, the EMM prefers tunneling at shorter R_{HO} values that are closer to the transition state. This is clearly the reason for the larger tunneling probabilities, leading in turn to a larger tunneling splitting.

To visualize the performance of the EMM as compared to that of the MM more globally, the semiclassical results are plotted versus the QM results in Figure 6 on a double logarithmic scale. The EMM results do systematically overestimate the QM results for splittings smaller than about 2 cm^{-1}. The correlation between MM and QM seems to be more erratic than that for EMM and QM. However, the absolute error of the log values (concerning all values shown in Figure 6) is similar, namely, 0.55 and 0.45 for MM and EMM, respectively. To show that there is a significant improvement concerning the EMM results, the log values for all splittings $\leq$ 2 cm^{-1} were fitted by a linear function, $f(x) = A + Bx$, with $x = \Delta$(QM). For MM and EMM, it was found that (A, B) = (0.5 $\pm$ 0.2, 1.3 $\pm$ 0.1) and (0.4 $\pm$ 0.1, 1.04 $\pm$ 0.05), respectively. For an exact correlation, one would expect (0, 1). Thus, the difference between the EMM and QM results is mainly the constant factor $10^{0.4} \approx 2.5$. This suggests immediately that a *calibration* of the results would be reasonable if certain exact splittings are known. As far as the MM splittings are concerned, there is a significant deviation from slope 1, and the results cannot be corrected by simply introducing a constant factor. For states with splittings larger than about 2 cm^{-1}, there are also underestimations by EMM. These states are rather highly excited; that is, the normal-mode sampling is less efficient, which is most likely a major source of error. Moreover, the quantum spectrum is dominated by a 2:3 Fermi resonance between the OH bend and the OO vibration.[31] This leads to a perturbation of the spectra that cannot be accounted for by the present semiclassical methods.

Finally, the results are analyzed with respect to the number of parities that were flipped. Figure 7 shows EMM tunneling splittings for selected fundamentals and overtones (cf. Table 1) and tunneling splittings that were obtained by keeping only those W_n values in the sum eq 8 for which there were, respectively, one ("1"), two ("2"), or three ("3") negative parities when the generalized trajectory crossed the symmetry surface Σ; the sum ("sum") corresponds to the values given in Table 1. The case of three negative parities is irrelevant. Surprisingly, both cases with one and two parities contribute equal amounts (in a logarithmic sense). For the two-dimensional symmetric coupling potential, the MM tunneling direction $\mathbf{d} = (-1, 0)^t$ becomes equivalent to one of the normal modes for vanishing coupling.[29] For the hydroperoxyl anion, however, the normal modes do not coincide with the definition of the straight line direction, eq 16. Thus, the reason for the better performance of the EMM for the

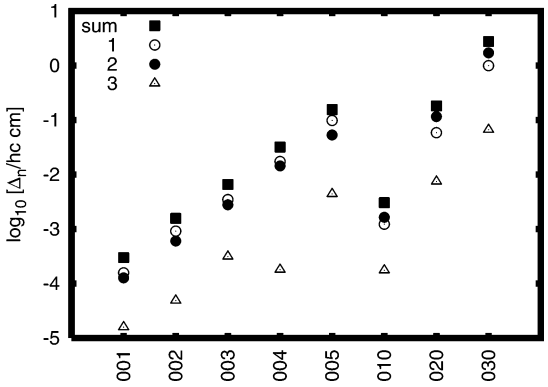

Figure 7. Mode-specific tunneling splittings Δ_n (logarithmic) obtained by the EMM: values for tunneling with one ("1"), two ("2"), and three ("3") parities and the sum ("sum") (cf. Table 1) are shown.

hydroperoxyl anion can be attributed to the more physical treatment of the connection condition of the semiclassical wave function across the caustic surfaces separating the regions of real, complex, and imaginary actions.

4. Conclusions

The recently proposed extension of the Makri−Miller model[29] has been applied to calculate tunneling splittings of vibrational modes for a three-dimensional ab initio potential energy surface describing the hydrogen-atom transfer in the hydroperoxyl anion.[32] For moderate excitation energies, it was found that the results of the extended Makri−Miller model systematically overestimate the quantum mechanical values, while the conventional Makri−Miller results show over- and underestimations in an erratic manner. It was pointed out that a calibration of the extended Makri−Miller method results by a constant factor is reasonable. It should be stressed that both methods rely on several ad hoc assumptions that can only be justified by numerical tests, as in this study. The present findings suggest that the extended Makri−Miller method gives a more realistic description of the connection of the semiclassical wave function across the different regions of configuration space. However, whether this feature is more general remains to be shown. Furthermore, it turned out that tunneling with one and two parity changes is almost equally important (in a logarithmic sense). This observation should be of high relevance for current attempts to use generalized trajectories for time-dependent wave-packet dynamics.[36]

Finally, the present method has to be brought into the context of ab initio molecular dynamics simulations with an on-the-fly calculation of the forces which has been used in connection with the Makri−Miller model.[26] Because the extended Makri−Miller method is trajectory-based as well, there seems to be no principal problem with an implementation of an ab initio molecular dynamics scheme. However, it should be emphasized that the benefits of this method come at the price of an increased numerical complexity. First, significantly more tunneling trajectories need to be calculated, and several of them are subsequently discarded. Second, the solution of Hamilton's equation of motion for the parity-based trajectories will typically require a smaller step size than the calculation of the potential energy along a straight line. Nevertheless, the present study shows that this new protocol may deserve further investigation.

Acknowledgment. This work was supported by the Deutsche Forschungsgemeinschaft (Project Ma 515/19-2). We would like to thank Dr. W.-T. Chan (Toronto) for providing the Fortran code for the potential energy surface, Prof. K. Takatsuka and Dr. H. Ushiyama (Tokyo) for helpful discussions, and Prof. J. Manz (Berlin) for his continued support of this work.

Note Added after ASAP Publication. This article was released ASAP on March 18, 2006, with the incorrect Received Date. The correct version was posted on April 12, 2006.

References

(1) Bell, R. P. *The Tunnel Effect in Chemistry*; Chapman and Hall: London, 1980.

(2) Benderskii, V. A.; Makarov, D. E.; Wright, C. A. *Adv. Chem. Phys.* **1994**, *88*, 1.

(3) Landau, L. D.; Lifshitz, E. M. *Quantum Mechanics*; Pergamon: Oxford, 1975.

(4) Delos, J. B. *Adv. Chem. Phys.* **1985**, *65*, 161.

(5) Huang, Z. H.; Feuchtwang, T. E.; Cutler, P. H.; Kazes, E. *Phys. Rev. A* **1990**, *41*, 32.

(6) Takada, S.; Nakamura, H. *J. Chem. Phys.* **1994**, *100*, 98.

(7) Takada, S.; Nakamura, H. *J. Chem. Phys.* **1995**, *102*, 3977.

(8) Tautermann, C. S.; Voegele, A. F.; Loerting, T.; Liedl, K. R. *J. Chem. Phys.* **2002**, *117*, 1967.

(9) Kleinert, H. *Path Integrals in Quantum Mechanics, Statistics, Polymer Physics, and Financial Markets*, 3rd ed.; World Scientific: New Jersey, 2004.

(10) Benderskii, V. A.; Grebenshchikov, S. Y.; Mil'nikov, G. V.; Vetoshkin, E. V. *Chem. Phys.* **1994**, *188*, 19.

(11) Benderskii, V.; Vetoshkin, E.; Irgibaeva, I.; Trommsdorff, H. *Chem. Phys.* **2000**, *262*, 393.

(12) Smedarchina, Z.; Fernandez-Ramos, A.; Siebrand, W. *J. Comput. Chem.* **2001**, *22*, 787.

(13) Smedarchina, Z.; Fernandez-Ramos, A.; Siebrand, W. *Chem. Phys. Lett.* **2004**, *395*, 339.

(14) Mil'nikov, G.; Nakamura, H. *J. Chem. Phys.* **2001**, *115*, 6881.

(15) Mil'nikov, G. V.; Yagi, K.; Taketsugu, T.; Nakamura, H.; Hirao, K. *J. Chem. Phys.* **2003**, *119*, 10.

(16) Mil'nikov, G. V.; Nakamura, H. *J. Chem. Phys.* **2005**, *122*, 124311.

(17) Mil'nikov, G. V.; Kühn, O.; Nakamura, H. *J. Chem. Phys.* **2005**, *123*, 074308.

(18) Miller, W. H. *J. Phys. Chem. A* **2001**, *105*, 2942.

(19) Mandelshtam, V. A.; Ovchinikov, M. *J. Chem. Phys.* **1998**, *108*, 9206.

(20) Shalashilin, D. V.; Child, M. S. *J. Chem. Phys.* **2001**, *114*, 9296.

(21) Giese, K.; Kühn, O. *J. Chem. Phys.* **2004**, *120*, 4207.

(22) Ben-Nun, M.; Martinez, T. J. *J. Chem. Phys.* **2000**, *112*, 6113.

(23) Makri, N.; Miller, W. H. *J. Chem. Phys.* **1989**, *91*, 4026.

(24) Sewell, T. D.; Guo, Y.; Thompson, D. L. *J. Chem. Phys.* **1995**, *103*, 8557.

(25) Guo, Y.; Li, S.; Thompson, D. L. *J. Chem. Phys.* **1997**, *107*, 2853.

(26) Ben-Nun, M.; Martinez, T. J. *J. Phys. Chem. A* **1999**, *103*, 6055.

(27) Guallar, V.; Gherman, B. F.; Miller, W. H.; Lippard, S. J.; Friesner, R. A. *J. Am. Chem. Soc.* **2002**, *124*, 3377.

(28) Guo, Y.; Thompson, D. L. *J. Phys. Chem. A* **2002**, *106*, 8374.

(29) Giese, K.; Ushiyama, H.; Kühn, O. *Chem. Phys. Lett.* **2003**, *371*, 681.

(30) Takatsuka, K.; Ushiyama, H.; Inoue-Ushiyama, A. *Phys. Rep.* **1999**, *322*, 347.

(31) Chan, W.-T.; Hamilton, I. P. *J. Chem. Phys.* **1996**, *105*, 5907.

(32) Chan, W.-T.; Hamilton, I. P. *Chem. Phys. Lett.* **1998**, *292*, 57.

(33) Maslov, V. P.; Fedoriuk, M. V. *Semiclassical Approximations in Quantum Mechanics*; D. Reidel: Dordrecht, The Netherlands, 1981.

(34) Gutzwiller, M. C. *Chaos in Classical and Quantum Mechanics*; Springer-Verlag: New York, 1990.

(35) Gray, S. K.; Noid, D. W.; Sumpter, B. G. *J. Chem. Phys.* **1994**, *101*, 4062.

(36) Ushiyama, H.; Takatsuka, K. *J. Chem. Phys.* **2004**, *120*, 4561.

CT0502918